SCIENCE CHINA Information Sciences



RESEARCH PAPER

Spintronic-metasurface terahertz emitters with magnetic-field manipulated polarizations

Qing YANG¹, Yan HUANG¹, Houyi CHENG^{1,2}, Jie ZHANG¹, Fan ZHANG^{1,2}, Yong XU^{1,3}, Lianggong WEN^{1,4}, Weisheng ZHAO^{1,2,3,4} & Tianxiao NIE^{1,2,3,4*}

¹MIIT Key Laboratory of Spintronics, School of Integrated Circuit Science and Engineering, Beihang University, Beijing 100191, China

²Hefei Innovation Research Institute, Beihang University, Hefei 230012, China
³National Key Lab of Spintronics, Institute of International Innovation, Beihang University, Hangzhou 311115, China
⁴Qingdao Innovation Research Institute, Beihang University, Qingdao 266000, China

Received 23 November 2024/Revised 20 February 2025/Accepted 13 May 2025/Published online 17 October 2025

Abstract The rapid development of information technologies for terahertz (THz) sensing, wireless communication, and low-dissipation quantum computation requires ultracompact and high-efficiency THz functional devices. Spintronic-metasurface emitters, which realize diverse polarization state modulation during THz wave generation, have illuminated a revolutionary avenue for the next-generation on-chip functional THz devices. Currently, broadband polarization modulation is achieved in spintronic-metasurface emitters through rotating setups and arranging patterns. However, there has been little study on the distribution of external magnetic fields for THz radiation. Here, we demonstrate that nonuniform magnetization contributes to achieving more diverse THz chirality in patterned emitters. The symmetry of THz radiation is broken when the azimuth angle of emitters exceeds 90°, providing an effective approach to achieve full ellipticity ranging from 0 to 0.85 over the 0.5–2.5 THz frequency band. Moreover, under curved magnetization, ellipticity exceeding 0.6 can be achieved in patterned emitters, where no chiral THz waves are radiated under a uniform magnetic field. Our findings provide the capability to expand the application scenarios of integrated spin-optoelectronic devices, shedding light on potential benefits in wireless communications and biomedical detection.

Keywords chiral terahertz waves modulation, spintronic terahertz emission, spintronic-metasurface THz emitters, the twisted magnetic field, broadband

Citation Yang Q, Huang Y, Cheng H Y, et al. Spintronic-metasurface terahertz emitters with magnetic-field manipulated polarizations. Sci China Inf Sci, 2025, 68(11): 212401, https://doi.org/10.1007/s11432-024-4440-9

1 Introduction

Terahertz (THz) radiation has inspired numerous promising applications in spectral imaging and noninvasive biomedical detection [1-6]. In particular, chiral terahertz technology holds great potential for significant impact in wireless communications [7–10], nondestructive testing [11–13], and biomedical sensing [14–18]. A great deal of research has been devoted to manipulating the electric-field vector of THz waves to achieve flexible control of their amplitude, phase, frequency, polarization and spatial properties flexibly [4, 19–24]. However, modulating THz waves typically relies on the insertion of optical elements, such as waveplates and liquid crystal, which results in low efficiency and a narrow manipulation bandwidth [25–29]. Therefore, there remains interest in exploring a valid way to modulate chiral THz waves [30–33]. Recently, integrating spintronic THz emitters into metasurface [34–44] has been shown to have the potential to manipulate broadband THz chirality at room temperature [45-48] in compact and multifunctional systems [43, 49-56]. In particular, magnetization distribution, the most decisive factor for the radiated THz polarization according to the inverse Hall effect (ISHE) [57–60], urgently needs to explore its impact on the generation of chiral THz waves. In this work, striped-array emitters are positioned at the center of an inhomogeneous magnetic field by opposing like poles of magnets. When these devices are rotated within the twisted magnetic field, they exhibit an asymmetry in amplitude and phase difference. This asymmetry results in a full range of ellipticity values from 0 to 0.85 across

^{*} Corresponding author (email: nietianxiao@buaa.edu.cn)

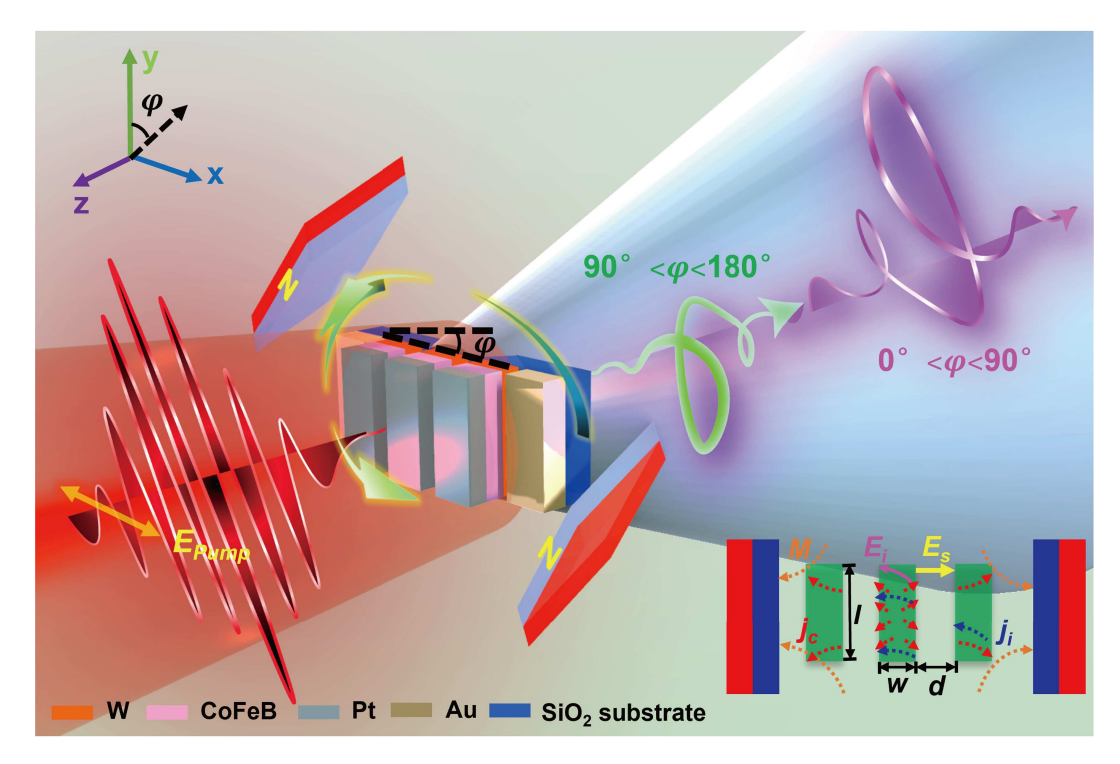


Figure 1 (Color online) Diagram of chiral terahertz generation and modulation. A femtosecond laser along the z axis is vertically incident on the patterned emitter surface with the fixed twisted magnetic field. Chiral terahertz waves with different ellipticity can be obtained when rotating them in the x-y plane by φ and $180^{\circ} - \varphi$. The inset illustrates that the twisted magnetic field would change the direction of j_c , E_i and j_i , which causes different diverse ellipticity modulation effect compared with the situation under uniform fields.

the 0.5–2.5 THz frequency range. Additionally, we achieve an ellipticity value greater than 0.6 in the emitter, even when only linearly polarized waves are present under uniform magnetic fields. Our findings address the gap in understanding how magnetization distribution influences spintronic-metasurface THz multifunctional devices. They contribute to a deeper comprehension of the modulation mechanisms of chiral THz waves and expand the repertoire of manipulation techniques for next-generation on-chip THz devices.

2 Materials and methods

Figure 1 shows the experimental schematic diagram for the radiation of chiral terahertz waves under a twisted magnetic field. A femtosecond (fs) laser with a central wavelength of 800 nm, a pulse duration of 35 fs, and a repetition rate of 1 kHz, generated by an amplified Ti:sapphire laser source, is used to excite the spin-metasurface device. The excitation pulse has a power of approximately 150 mW, and the beam radius at the metasurface emitter is approximately 1 cm. The electric field direction of the pump laser is aligned along the x-axis. Under fs laser illumination, the longitudinal spin current j_s arising in the ferromagnetic (FM) layer is converted into a transverse charge current j_c due to ISHE. The conversion relationship between two currents is $j_c = \gamma j_s \times M/|M|$, where M is the magnetization and γ is the spin-Hall angle of the nonferromagnetic (NM) layers [61,62]. The spintronic-metasurface emitter consists of striped-patterned trilayer heterostructures of W (5 nm)/CoFeB (2 nm)/Pt (2 nm) nanofilms, which are grown on a 500 µm thick SiO₂ substrate in a direct current (DC) and radio frequency (RF) sputtering system. In our experiment, five groups of metasurface structures with different aspect ratio (l:w) are selected: D0 (1:1), D1 (10:1), D2 (20:1), D3 (30:1) and D4 (50:1), while the value of l/d remains constant at 5.66:1. Each group comprises 22 strips, with each stripe maintaining the same area of 20000 μ m². In this experiment, we initially align the stripes along the z axis and then rotate them in the xy plane by an angle φ to get polarization modulation. The azimuth angle φ is defined as the angle between the emitters and the y axis.

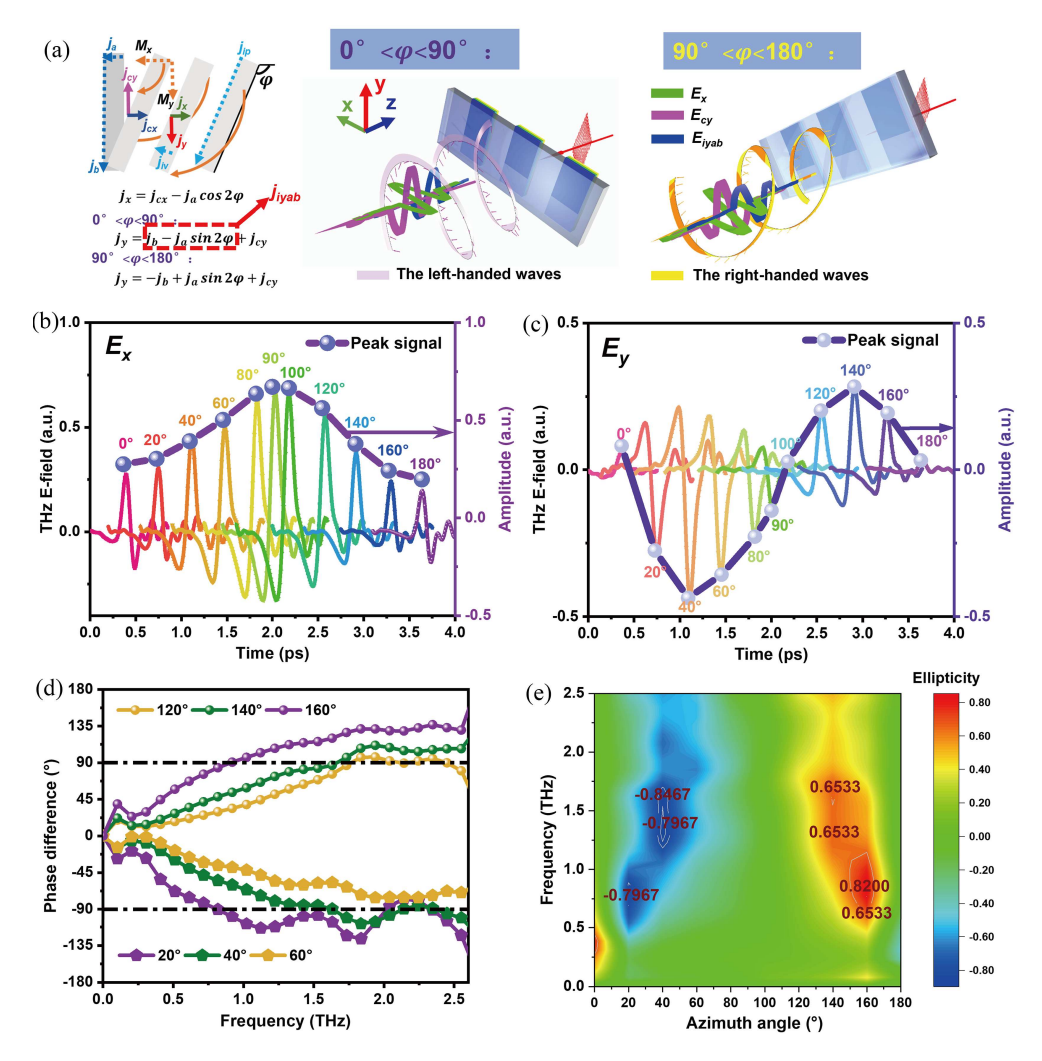


Figure 2 (Color online) Manipulation of terahertz chirality by rotating D4 under the twisted magnetic field distribution. (a) The concept sketch of the manipulation of the terahertz chirality by rotating azimuth angles of devices. In the left picture, the pink component is the THz E-field of j_{cy} , which comes from the component in the x direction of the external magnetic field due to the inverse spin Hall effect (ISHE). Similarly, j_{cx} also originates from M_x . Under the effect of the backflow j_i , the current density in the x and y directions is donated as j_x and j_y . In the middle and the right subfigures, the purple curve presents the left-handed waves and the yellow is the right-handed waves. The THz E-fields of j_x are represented in green. In order to more vividly illustrate the causes for asymmetry, we represent E_{cy} and E_{iyab} in the purplish red and red curves. (b) and (c) The THz amplitudes in the x and y directions as a function of the azimuth angles φ . The signals have been horizontally offset for clarity. (d) The phase difference between E_x and E_y . (e) The ellipticities change with different azimuth angles.

3 Results and discussion

As shown in the inserted picture, under the non-uniform magnetic field distribution, the spin-converted in-plane transverse ultrafast charge current j_c is generated, with its predominant flow directions perpendicular to the corresponding dominant magnetic fields [60]. The charge current j_c results in charge accumulation at all boundaries of a stripe, forming the non-uniform built-in electric field E_i . Meanwhile, a uniform gap electric field E_s is generated between adjacent stripes due to the similar arrangement of charges on adjacent boundaries. When the component of E_i in the direction of stripe arrangement exceeds E_s , charges can no longer remain at the boundaries of the stripes. Similarly, the charges on the other two sides of the stripe also cannot remain at the boundaries. We define the currents in a stripe induced by these two electric fields as the backflow j_i . j_i will suppress the amplitude of the original current, change its phase and cause diverse ellipticity modulation effects.

Generating elliptical THz waves is the result of the combined effects of the azimuth angle and magnetization [63]. The influence of external inhomogeneous magnetic fields on chiral THz radiation is clearly illustrated in Figure 2(a). The magnetic moments along the x and y directions are defined as M_x and M_y , respectively. According to ISHE, the components of j_c in the x and y directions, recorded as j_{cx}

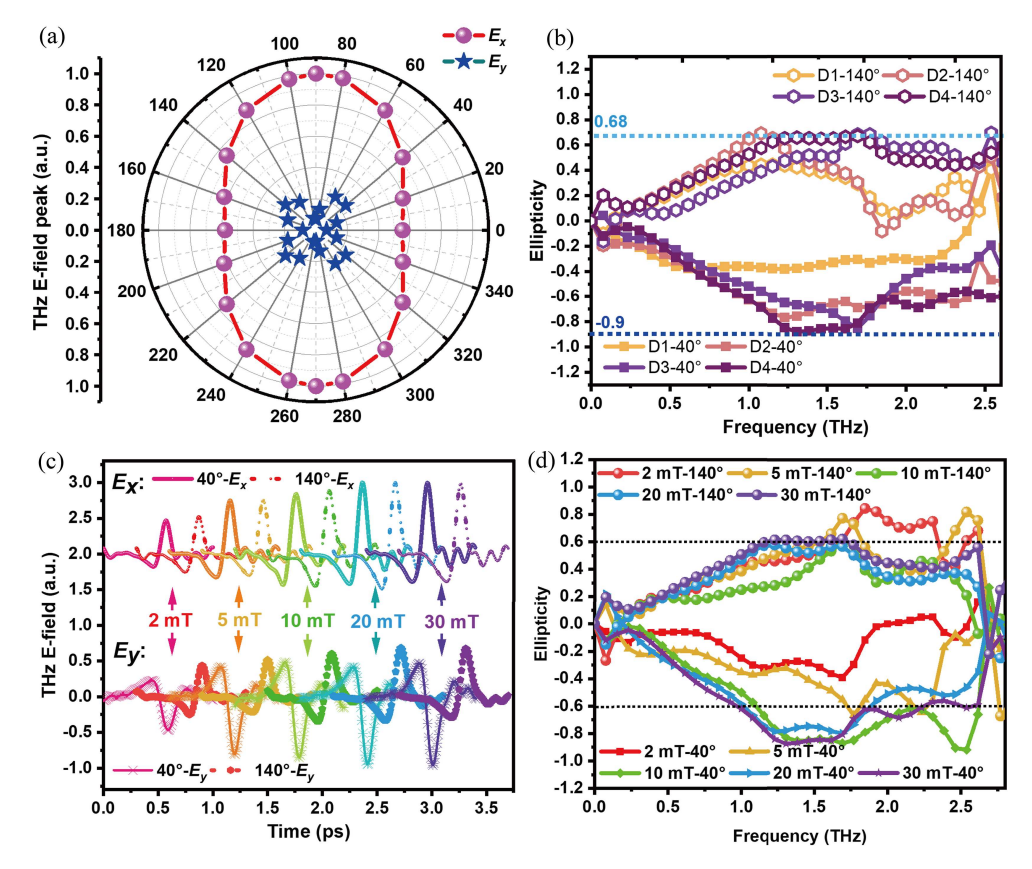


Figure 3 (Color online) Performance of the backflow, the built-in electric field and applied magnetic field on polarization modulation. (a) Amplitude in the x and y directions from the rotation of a conductive striped-array emitter with an aspect ratio 50:1 under 30 mT nonuniform magnetic field; (b) ellipticity modulation results of several patterned emitters with different aspect ratios under 30 mT nonuniform magnetic field; (c) amplitude in the x and y directions of D4 under different strength twisted magnetic fields; (d) ellipticity modulation results in D4 under different strength twisted magnetic fields.

and j_{cy} , are perpendicular to M_x and M_y , respectively. We define the component of j_c in the x and y directions, which are affected by j_i , as j_x and j_y , respectively. These components are represented by green and red in the middle and the right subfigures of Figure 2(a). Here, to visually represent the direction of the backflow, j_i is divided into j_{iv} and j_{ip} , which are perpendicular and parallel to the direction of stripe arrangement, respectively. We define j_{iv} and j_{ip} at the initial moment as j_a and j_b , respectively. Owing to the change in the number of accumulating charges on boundaries when rotating the device, we use j_a and j_b to calculate the current change during the device's rotation. A chiral THz beam undergoes a change from left-handed to right-handed polarization at φ and $180^{\circ} - \varphi$ due to a phase reversal in the y-component of backflow. Through current decomposition, we found that j_{cy} is responsible for the broken symmetry of E_y , as well as the phase. The detailed current analysis is shown in the Supporting Information Section S2. Here, we rotate D4 under a 30 mT twisted magnetic field to verify the above statement. As shown in Figures 2(b) and (c), the phase reversal in the y direction enables the switching between left-handed and right-handed waves. The amplitude in the y-direction also exhibits significant asymmetry after a 90° rotation. A similar phenomenon is also observed in the phase difference in the frequency domain, as shown in Figure 2(d). This reveals that chirality asymmetry is distributed across a wide frequency range. Additionally, the tunable ellipticity during azimuth rotation, summarized in Figure 2(e), demonstrates that a twisted magnetic field enables patterned emitters to achieve full ellipticity from 0 to 0.85 over the frequency range of 0.5 to 2.5 THz. This capability paves a new path for diverse polarization modulation in integrated THz optoelectronic devices.

It has been reported that switching between linear and elliptical polarization states can be achieved in FM/NM films by tailoring the magnetization distributions [60]. Here, we employ a conductive patterned emitter with a 50:1 aspect ratio to demonstrate that the chirality in patterned terahertz sources originates from charge accumulation, which is distinct from that in thin films. As displayed in Figure 3(a), the weak THz amplitude of E_y does not follow an angle-dependent model in the conductive patterned emitter. This

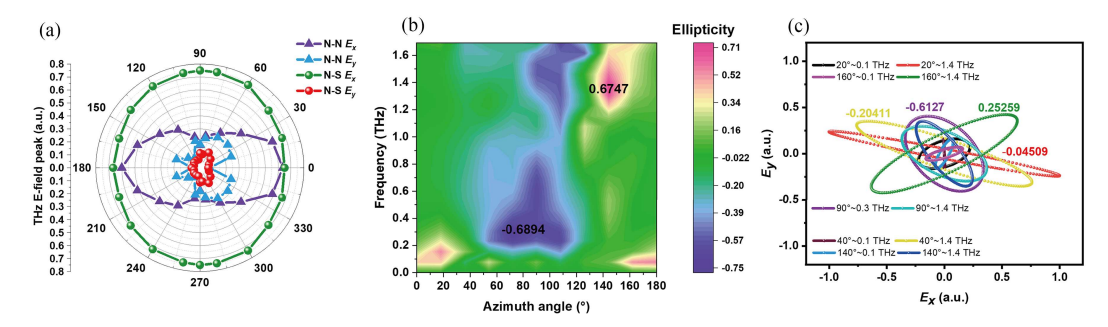


Figure 4 (Color online) Broadband polarization state modulation is achieved in D0 only under the twisted magnetic field. (a) The amplitude in the x and y directions comparison of D0 between under a uniform magnetic field and a twisted field. The amplitude of two magnetic fields is the same as 30 mT. (b) The ellipticities change with different azimuth angles. (c) The electric fields of the radiated waves for D0, illustrating the capability to manipulate polarization states and chirality.

is because the tungsten layer is conductive, preventing most charges from accumulating at the edges. Consequently, there is no strong E_i to drag charges and form j_i , resulting in the generation of linearly polarized waves at any azimuth. We also investigated the impact of stripe size on the modulation of chiral THz waves. Figure 3(b) systematically compares the modulation effect of D1-D4 at 40° and 140°, showing that the larger aspect ratio is conducive to achieving greater ellipticity and exacerbating the asymmetry of polarization states over a broadband range. In particular, within the 1.2 to 1.6 THz frequency range, the ellipticity of D4 remains above 0.8 at 40° and stabilizes around 0.65 at 140°. Although the maximum value of ellipticity does not increase significantly with the increasing aspect ratio at the same azimuth angle, the frequency range covered becomes progressively wider. It is evident that large aspect ratios contribute to achieving broadband chiral terahertz modulation. The asymmetry of polarization states is also closely related to the magnetic field strength. As shown in Figure 3(c), the emission amplitude varies with the magnetic strength, which is adjusted by changing the number of static magnets. This reveals that the intensification of symmetry breaking can be achieved through a stronger twisted magnetic field. The ellipticity distribution in the frequency domain can reveal the polarization dependence of THz emission on the varying external magnetic field. As shown in Figure 3(d), a larger magnetic field makes the difference of the modulation of chirality at 40° and 140° more pronounced. Moreover, the diversity of polarization state modulation can also be affected by the twisted magnetic field. When φ is 140°. the increase in the magnetic field's amplitude has no apparent distinguished effect on ellipticity, which is significantly different from the effect at 40°. When the external magnetic field strength exceeds 10 mT, the amplitude of the x and y components at the same azimuth angle, as well as the ellipticity distribution in the frequency domain, remain largely constant with further increases in magnetic field strength. This phenomenon can be attributed to the device's relatively small coercive field of approximately 10 mT. These findings suggest that our device can maintain stable performance across different magnetization environments.

In order to comprehensively characterize the manipulation performance of twisted magnetic fields on spintronic-metasurface THz emitters for radiating chiral THz waves, a striped-array device with an aspect ratio of l:w=1:1 for tunable polarization states is utilized here. As shown in Figure 4(a), D0 exhibits a clear angle dependence of amplitude in the x and y direction under a 30 mT twisted magnetic field, which is distinct from the behavior observed under uniform magnetization. Figure 4(b) presents the measured rotation of the azimuth for different ellipticities in the frequency domain. Throughout the entire rotation process, the maximum ellipticity of around 0.68 is achieved at 0.2–0.4 THz for angles from 60° to 120°, and at 1.2–1.4 THz from 140° to 160°. The generated polarized THz spectra at several selected frequencies (0.1 THz or 0.3 THz and 1.4 THz) at $\varphi = 20^{\circ}$, 90° and 160° are summarized in Figure 4(c). At the frequencies we are considering, the variation of ellipticities with different azimuth angles demonstrates the ability of the twisted magnetic field to modulate elliptical THz waves in both the low and high frequency bands. This modulation also enhances the chirality control of the spintronic-metasurface device, even with a weak E_i .

4 Conclusion

In this work, we demonstrate the manipulation of both the chirality and ellipticity of the generated

elliptical terahertz waves by rotating the trilayer heterostructures, which are fabricated into micrometerscale stripes under an applied nonuniform magnetic field distribution. The built-in electric fields and the magnetic strength both play crucial roles in affecting the terahertz amplitude and phase difference between the x and y directions, thereby enabling modulation of polarization states. Notably, the twisted magnetic field induces an asymmetry when the azimuth angle of emitters exceeds 90° , which endows the potential to achieve full polarization over a wide frequency band. More significantly, the twisted magnetic field compensates for the deficiency that elliptical THz waves can be achieved in the patterned emitter with a small strength built-in electric field. We believe that this work will pave a novel path toward the development of various on-chip THz multifunctional devices, which will play important roles in future fundamental sciences and practical applications.

Acknowledgements This work was supported by National Key R&D Program of China (Grant Nos. 2024YFA1408800, 2023YFF0719200, 2023YFF0717500, 2022YFA1402604, 2021YFB3601303), National Natural Science Foundation of China (Grant Nos. W2411060, 62274009, 52003014), Beijing Municipal Natural Science Foundation (Grant No. Z230004), Natural Science Foundation for the Youth (Grant No. 62105011), Guangdong Basic and Applied Basic Research Foundation (Grant No. 2021B1515120012), Science and Technology Benefit for the People Demonstration Special Project of Qingdao (Grant No. 23-2-8-smjk-3-nsh), Taishan Industry Leading Talents (tscx202306030), and Key R&D Program of Shandong Province (Grant No. 2022ZDPT01).

Supporting information Appendixes A–D. The supporting information is available online at info.scichina.com and link. springer.com. The supporting materials are published as submitted, without typesetting or editing. The responsibility for scientific accuracy and content remains entirely with the authors.

References

- 1 Nikoo M S, Matioli E. Electronic metadevices for terahertz applications. Nature, 2023, 614: 451-455
- 2 Tuniz A, Kuhlmey B T. Subwavelength terahertz imaging via virtual superlensing in the radiating near field. Nat Commun, 2023, 14: 6393
- 3 Stantchev R I, Yu X, Blu T, et al. Real-time terahertz imaging with a single-pixel detector. Nat Commun, 2020, 11: 2535
- 4 Schlauderer S, Lange C, Baierl S, et al. Temporal and spectral fingerprints of ultrafast all-coherent spin switching. Nature, 2019, 569: 383–387
- 5 Ferguson B, Zhang X C. Materials for terahertz science and technology. Nat Mater, 2002, 1: 26–33
- 6 Chen X, Wang H, Wang C, et al. Efficient generation and arbitrary manipulation of chiral terahertz waves emitted from Bi₂Te₃-Fe heterostructures. Adv Photon Res, 2021, 2: 2000099
- 7 Nagai Y, Guo J, Sumi T, et al. Improve IEEE 802.15.4 network reliability by suspendable CSMA/CA. In: Proceedings of IEEE Wireless Communications and Networking Conference (WCNC), 2024. 1–6
- 8 Zhang R, Guo Y, Zhang F, et al. Dual-layer metasurface enhanced capacity of polarization multiplexing. Laser Photon Rev, 2024, 18: 2400126
- 9 Yu Z, Gao X, Yao J, et al. A spatial-frequency patching metasurface enabling super-capacity perfect vector vortex beams. eLight, 2024, 4: 21
- 10 Song Q, Zhou Z W, Xu Y F, et al. Low-bias, high-photoresponsivity SnSe₂ nanofilm with an Au split-ring array-based THz detector toward 6G communication. Sci China Inf Sci, 2023, 66: 169405
- 11 Hu X, Wang X, Hu H, et al. Terahertz reflective imaging systems with improved angle compatibility realized by the designed quasi-scattering screen. Optics Laser Tech, 2024, 176: 110913
- 12 Lu R, Li Y, Song H, et al. Recent advances in emerging polarization-sensitive materials: from linear/circular polarization detection to neuromorphic device applications. Adv Funct Mater, 2025, 35: 2423770
- 13 Meng Y, Feng J, Han S, et al. Photonic van der Waals integration from 2D materials to 3D nanomembranes. Nat Rev Mater, 2023, 8: 498-517
- 14 Huang Y, Shen Y, Wang J. From terahertz imaging to terahertz wireless communications. Engineering, 2023, 22: 106-124
- 15 Koch M, Mittleman D M, Ornik J, et al. Terahertz time-domain spectroscopy. Nat Rev Methods Primers, 2023, 3: 48
- 16 Ma L, Shi W, Fan F, et al. Terahertz polarization sensing, chirality enhancement, and specific binding based on metasurface sensors for biochemical detection: a review. Chin Opt Lett, 2023, 21: 110003
- 17 Blackburn T J, Tyler S M, Pemberton J E. Optical spectroscopy of surfaces, interfaces, and thin films. Anal Chem, 2022, 94: 515–558
- 18 Khan S A, Khan N Z, Xie Y, et al. Optical sensing by metamaterials and metasurfaces: from physics to biomolecule detection. Adv Opt Mater, 2022, 10: 2200500
- 19 Ulbricht R, Hendry E, Shan J, et al. Carrier dynamics in semiconductors studied with time-resolved terahertz spectroscopy. Rev Mod Phys, 2011, 83: 543–586
- 20 Kampfrath T, Tanaka K, Nelson K A. Resonant and nonresonant control over matter and light by intense terahertz transients. Nat Photon, 2013, 7: 680–690
- 21 Liu M, Hwang H Y, Tao H, et al. Terahertz-field-induced insulator-to-metal transition in vanadium dioxide metamaterial. Nature, 2012, 487: 345–348
- 22 Yang S J, Peng Y Z, Lyu W T, et al. Near-field channel estimation for extremely large-scale terahertz communications. Sci China Inf Sci, 2024, 67: 192302
- 23 Cui M Y, Dai L L. Near-field wideband channel estimation for extremely large-scale MIMO. Sci China Inf Sci, 2023, 66: 172303
- 24 Xu J D, Yuen C C, Huang C W, et al. Reconfiguring wireless environments via intelligent surfaces for 6G: reflection, modulation, and security. Sci China Inf Sci, 2023, 66: 130304
- 25 Shan J, Dadap J I, Heinz T F. Circularly polarized light in the single-cycle limit: The nature of highly polychromatic radiation of defined polarization. Opt Express, 2009, 17: 7431–7439
- 26 Masson J B, Gallot G. Terahertz achromatic quarter-wave plate. Opt Lett, 2006, 31: 265-267
- 27 Yang C S, Tang T T, Chen P H, et al. Voltage-controlled liquid-crystal terahertz phase shifter with indium C tin C oxide nanowhiskers as transparent electrodes. Opt Lett, 2014, 39: 2511–2513
- Zeng H, Liang H, Zhang Y, et al. High-precision digital terahertz phase manipulation within a multichannel field perturbation coding chip. Nat Photon, 2021, 15: 751–757
- 29 Yang Q, Sun T, Wu X, et al. Fast tunable biological fluorescence detection device with integrable liquid crystal filter. Crystals, 2021, 11: 272

- Tong M, Hu Y, He W, et al. Light-driven spintronic heterostructures for coded terahertz emission. ACS Nano, 2022, 16: 8294-8300
- Wang S, Qin W, Zhang S, et al. Nanoengineered spintronic-metasurface terahertz emitters enable beam steering and full polarization control. Nano Lett, 2022, 22: 10111-10119
- Li J, Yuan Y, Wu Q, et al. Bi-isotropic Huygens' metasurface for polarization-insensitive cross-polarization conversion and wavefront manipulation. IEEE Trans Antennas Propagat, 2024, 72: 2445–2454
- Yuan Y, Zhou W, Zhang H, et al. Full-polarimetric synthesized holographic displaying empowered by chirality-assisted metasurface. Small Sci, 2024, 4: 2400138
- Li J. Hu G. Shi L, et al. Full-color enhanced second harmonic generation using rainbow trapping in ultrathin hyperbolic metamaterials. Nat Commun, 2021, 12: 6425
- Huang Z, Zheng Y, Li J, et al. High-resolution metalens imaging polarimetry. Nano Lett, 2023, 23: 10991-10997
- Feng S, Yang L, Cai B, et al. Tri-band terahertz metamaterial absorber based on structural ${\rm Ti}_3{\rm C}_2{\rm T}_x$ MXene for enhanced sensing application. IEEE Sens J, 2024, 24: 28889–28896
- Cheng Y, Xing R, Chen F, et al. Terahertz pseudo-waveform-selective metasurface absorber based on a square-patch structure loaded with linear circuit components. Adv Photon Res, 2024, 5: 2300303
- Yang W, Yang L, Cai B, et al. Efficiency tunable terahertz graphene metasurfaces for reflective single/dual-focusing effects based on Pancharatnam-Berry phase. Results Phys, 2024, 65: 108003
- Chen J, Zhang W, Yang W, et al. Separation of benzene and toluene associated with vapochromic behaviors by hybrid[4]arenebased co-crystals. Nat Commun, 2024, 15: 1260
- Deng M, Kanwal S, Wang Z, et al. Dielectric metasurfaces for broadband phase-contrast relief-like imaging. Nano Lett, 2024, 40 24: 14641-14647
- Song Y, Qiu C, Zhou H, et al. Mechanisms and models of interface trap annealing in positively-biased MOS devices. J Phys 41 D-Appl Phys, 2024, 58: 025109
- Yuan Y, Zhang K, Wu Q, et al. Reaching the efficiency limit of arbitrary polarization transformation with non-orthogonal metasurfaces. Nat Commun, 2024, 15: 6682
- Li J T, Yue Z, Li J, et al. Diverse terahertz wavefront manipulations empowered by the spatially interleaved metasurfaces. Sci China Inf Sci, 2023, 66: 132301
- Wang B, Yuan J, Che M Q, et al. High-performance broadband photodetector based on PtSe₂/MoS₂ heterojunction from visible to near-infrared region. Sci China Înf Sci, 2024, 67: 132401
- 45 Liu C. Wang S. Zhang S. et al. Active spintronic-metasurface terahertz emitters with tunable chirality. Adv Photon. 2021, 3: 056002
- Sun T, Bai Z, Li Z, et al. Generation of tunable terahertz waves from tailored versatile spintronic meta-antenna arrays. ACS 46 Appl Mater Interfaces, 2023, 15: 23888–23898
- Yang D, Liang J, Zhou C, et al. Powerful and tunable THz emitters based on the Fe/Pt magnetic heterostructure. 2016. 47 ArXiv:1607.02814
- Zhao H, Chen X, Ouyang C, et al. Generation and manipulation of chiral terahertz waves in the three-dimensional topological insulator Bi₂Te₃. Adv Photon, 2020, 2: 066003
- 49 Cai X, Tang R, Zhou H, et al. Dynamically controlling terahertz wavefronts with cascaded metasurfaces. Adv Photon, 2021,
- Cong L, Srivastava Y K, Zhang H, et al. All-optical active THz metasurfaces for ultrafast polarization switching and dynamic beam splitting. Light Sci Appl, 2018, 7: 28
- Grady N K, Heyes J E, Chowdhury D R, et al. Terahertz metamaterials for linear polarization conversion and anomalous refraction. Science, 2013, 340: 1304-1307
- Jia M, Wang Z, Li H, et al. Efficient manipulations of circularly polarized terahertz waves with transmissive metasurfaces.
- Light Sci Appl, 2019, 8: 16
 Han Z, Ohno S, Tokizane Y, et al. Off-resonance and in-resonance metamaterial design for a high-transmission terahertz-wave quarter-wave plate. Opt Lett, 2018, 43: 2977–2980
- Wu Y, Elyasi M, Qiu X, et al. High performance THz emitters based on ferromagnetic/nonmagnetic heterostructures. 2016. ArXiv:1610.07020
- Liu W, Wang S R, Dai J Y, et al. Arbitrarily rotating polarization direction and manipulating phases in linear and nonlinear ways using programmable metasurface. Light Sci Appl, 2024, 13: 172
- Xu Z, Yang J, Song Z. Terahertz switchable metasurface for polarization conversion and hologram manipulation. Optics Lasers Eng, 2025, 184: 108641
- Seifert T S, Jaiswal S, Barker J, et al. Femtosecond formation dynamics of the spin Seebeck effect revealed by terahertz spectroscopy. Nat Commun, 2018, 9: 2899
- Zhou C, Liu Y P, Wang Z, et al. Broadband terahertz generation via the interface inverse Rashba-Edelstein effect. Phys Rev 58 Lett. 2018, 121: 086801
- Cheng L, Wang X, Yang W, et al. Far out-of-equilibrium spin populations trigger giant spin injection into atomically thin
- MoS_2 . Nat Phys, 2019, 15: 347–351 Kong D, Wu X, Wang B, et al. Broadband spintronic terahertz emitter with magnetic-field manipulated polarizations. Adv Opt Mater, 2019, 7: 1900487
- Kampfrath T, Battiato M, Maldonado P, et al. Terahertz spin current pulses controlled by magnetic heterostructures. Nat Nanotech, 2013, 8: 256–260
- Wang H, Wu H, Zhang J, et al. Room temperature energy-efficient spin-orbit torque switching in two-dimensional van der Waals Fe₃GeTe₂ induced by topological insulators. Nat Commun, 2023, 14: 5173
- Yang Q, Huang Y, Cheng H, et al. Broadband polarization spectrum tuning enabled by the built-in electric field of patterned spintronic terahertz emitters. Adv Photon, 2025, 7: 026007